

# Standardised uptake values from PET/CT images: comparison with conventional attenuation-corrected PET

M. Souvatzoglou<sup>1</sup>, S. I. Ziegler<sup>1</sup>, M. J. Martinez<sup>1</sup>, R. Busch<sup>2</sup>, G. Dzewas<sup>1</sup>, M. Schwaiger<sup>1</sup>, F. Bengel<sup>1</sup>

<sup>1</sup> Nuklearmedizinische Klinik der Technischen Universität München, Ismaninger Strasse 22, 81675 Munich, Germany

<sup>2</sup> Institut für Epidemiologie und Statistik der Technischen Universität München, Munich, Germany

Received: 21 December 2005 / Accepted: 29 May 2006 / Published online: 5 September 2006

© Springer-Verlag 2006

**Abstract. Purpose:** In PET/CT, CT-derived attenuation factors may influence standardised uptake values (SUVs) in tumour lesions and organs when compared with stand-alone PET. Therefore, we compared PET/CT-derived SUVs intra-individually in various organs and tumour lesions with stand-alone PET-derived SUVs.

**Methods:** Thirty-five patients with known or suspected cancer were prospectively included. Sixteen patients underwent FDG PET using an ECAT HR+scanner, and subsequently a second scan using a Biograph Sensation 16PET/CT scanner. Nineteen patients were scanned in the reverse order. All images were reconstructed with an iterative algorithm (OSEM). Suspected lesions were grouped as paradiaphragmatic versus distant from the diaphragm. Mean and maximum SUVs were also calculated for brain, lung, liver, spleen and vertebral bone. The attenuation coefficients ( $\mu$  values) used for correction of emission data (bone, soft tissue, lung) in the two data sets were determined. A body phantom containing six hot spheres and one cold cylinder was measured using the same protocol as in patients.

**Results:** Forty-six lesions were identified. There was a significant correlation of maximum and mean SUVs derived from PET and PET/CT for 14 paradiaphragmatic lesions ( $r=0.97$  respectively;  $p<0.001$  respectively) and for 32 lesions located distant from the diaphragm ( $r=0.87$  and  $r=0.89$  respectively;  $p<0.001$  respectively). No significant differences were observed in the SUVs calculated with PET and PET/CT in the lesions or in the organs. In the phantom, radioactivity concentration in spheres calculated from PET and from PET/CT correlated significantly ( $r=0.99$ ;  $p<0.001$ ).

**Conclusion:** SUVs of cancer lesions and normal organs were comparable between PET and PET/CT, supporting the usefulness of PET/CT-derived SUVs for quantification of tumour metabolism.

**Keywords:** Positron emission tomography – Standardised uptake value – Attenuation correction – Respiratory movement – Treatment response evaluation

**Eur J Nucl Med Mol Imaging (2007) 34:405–412**

DOI 10.1007/s00259-006-0196-1

## Introduction

Positron emission tomography (PET) has achieved an established role in the staging and restaging of many malignancies [1, 2]. However, there is also increasing evidence of its usefulness in treatment monitoring and the prediction of response or non-response. This allows risk stratification of patients and appropriate tailoring of therapy [3–6]. Particularly in lymphoma and oesophageal carcinoma, the benefit of such metabolic monitoring has recently been demonstrated [7–11].

Standardised uptake values (SUVs), calculated in conventional PET through transmission measurements (for review see [12]), are commonly used to measure therapy-induced changes in tumour glucose utilisation quantitatively. A potential problem in the present era of combined PET/CT scanners is that SUVs may not necessarily show the same absolute values and the same degree of reliability as those obtained from stand-alone PET scanners, in which attenuation correction factors are calculated using external 511-keV rod sources. In PET/CT, X-ray CT is used to obtain attenuation coefficients for the correction of emission data [13]. Differences in temporal and spatial resolution between the two scans can result in misregistration, especially for moving organs/lesions. Consequently, application of inappropriate attenuation coefficients ( $\mu$  values) may lead to differences in the calculated SUVs and compromise the reliability of metabolic quantification. Additionally, the use of CT-derived  $\mu$  values may influence absolute SUVs if transformation from the lower X-ray photon energy to 511 keV is not adequate.

These potential influences on SUVs could have an impact on the use of cutoff values which have been

M. Souvatzoglou (✉)  
Nuklearmedizinische Klinik der Technischen Universität München,  
Ismaninger Strasse 22,  
81675 Munich, Germany  
e-mail: msouvatz@t-online.de  
Tel.: +49-89-41402972, Fax: +49-89-41404841

previously established using stand-alone PET systems to predict therapy response [9–11, 14]. The aim of this prospective study was therefore to determine the correlation between SUVs derived from stand-alone PET and from PET/CT.

## Materials and methods

### *Patient population*

The study population comprised 35 patients (27 male and 8 female, mean age  $60.4 \pm 10.7$  years, range 39–85 years) referred for whole-body  $^{18}\text{F}$ -fluorodeoxyglucose (FDG) PET for clinical staging of malignancy. Thirty-two patients had oesophageal cancer, two had thyroid carcinoma and one had lymphoma. All patients agreed to undergo scans on both available camera systems, directly following each other. Sixteen were scanned first using stand-alone PET and then using PET/CT, while 19 were scanned first using PET/CT and then, PET. Prior to imaging, all patients gave written informed consent.

### *Data acquisition*

FDG was synthesised by a modified method of Hamacher et al. [15]. The injected dose was adjusted to body surface area ( $400 \text{ MBq}/1.74 \text{ m}^2$ ). Patients were injected with  $396 \pm 51.8 \text{ MBq}$  of FDG after 6 h of fasting. None of the patients were diabetic or had a fasting blood glucose level above  $120 \text{ mg/dl}$ .

For stand-alone PET imaging an ECAT HR+ scanner (Siemens) was used. This BGO-crystal tomograph has a 15.5-cm axial field of view and yields 63 image planes per bed position, 2.46 mm apart. Transaxial and axial resolution using a ramp filter are 4.9 and 5.2 mm full-width at half-maximum (FWHM) respectively [16]. Following emission imaging in two-dimensional (2D) mode (8 min per bed position;  $128 \times 128$  matrix), a post-injection radionuclide transmission scan with approximately 30 million counts per bed position was obtained using three rotating  $^{68}\text{Ge}$  rod sources.

PET/CT imaging was done using a Biograph Sensation 16 scanner (Siemens), which incorporates an ACCEL PET camera and a 16-slice multidetector CT. The ACCEL PET camera has LSO crystals and a 16.2-cm axial field of view and yields 47 image planes per bed position, 3.37 mm apart. Transaxial and axial resolution using a ramp filter is 6.3 and 6.5 mm FWHM respectively [16]. Prior to emission imaging (3 min per bed position,  $128 \times 128$  matrix), which was performed in three-dimensional mode (3D), a “low-dose” CT scan was acquired using the same axial coverage as for PET. Patients were asked to breathe shallowly and to hold their breath during the CT scan of the thorax and the upper abdomen without changing the respiratory level when the breath-hold command was heard. The CT tube parameters used were 120 keV and 26 mA. No contrast agent was applied.

Patients who first underwent PET and then PET/CT had their first scan at  $81.9 \pm 13.5 \text{ min p.i.}$  and their second scan at  $178.5 \pm 29.6 \text{ min p.i.}$ , while patients with the opposite acquisition order had PET/CT at  $67.9 \pm 12.4 \text{ min p.i.}$  and PET at  $122.7 \pm 26.5 \text{ min p.i.}$

### *Image reconstruction*

The emission data obtained in the conventional PET scanner were corrected for randoms, dead time and attenuation. Segmented photon

attenuation correction from the  $^{68}\text{Ge}$  transmission scan was applied to reduce noise from count-limited transmission data in the reconstructed PET images [17, 18]. An iterative reconstruction algorithm based on ordered-subset expectation maximisation (OSEM) with four iterations and eight subsets was applied for both the emission and the transmission scan. OSEM images underwent a 5-mm FWHM Gaussian post smoothing and were zoomed with a factor of 1.2; the pixel size of the reconstructed images was 4.3 mm.

Concerning the images obtained with PET/CT, CT data were converted from Hounsfield units (HU) to linear attenuation coefficients for 511 keV using a single CT energy scaling method based on a bilinear transformation, as described in the literature [13]. Emission data were corrected for randoms, dead time, scatter [19] and attenuation and the same reconstruction algorithm was applied as for the conventional PET data. The images were zoomed with a factor of 1.23, resulting in an identical image pixel size as for the conventional PET images.

### *Phantom studies*

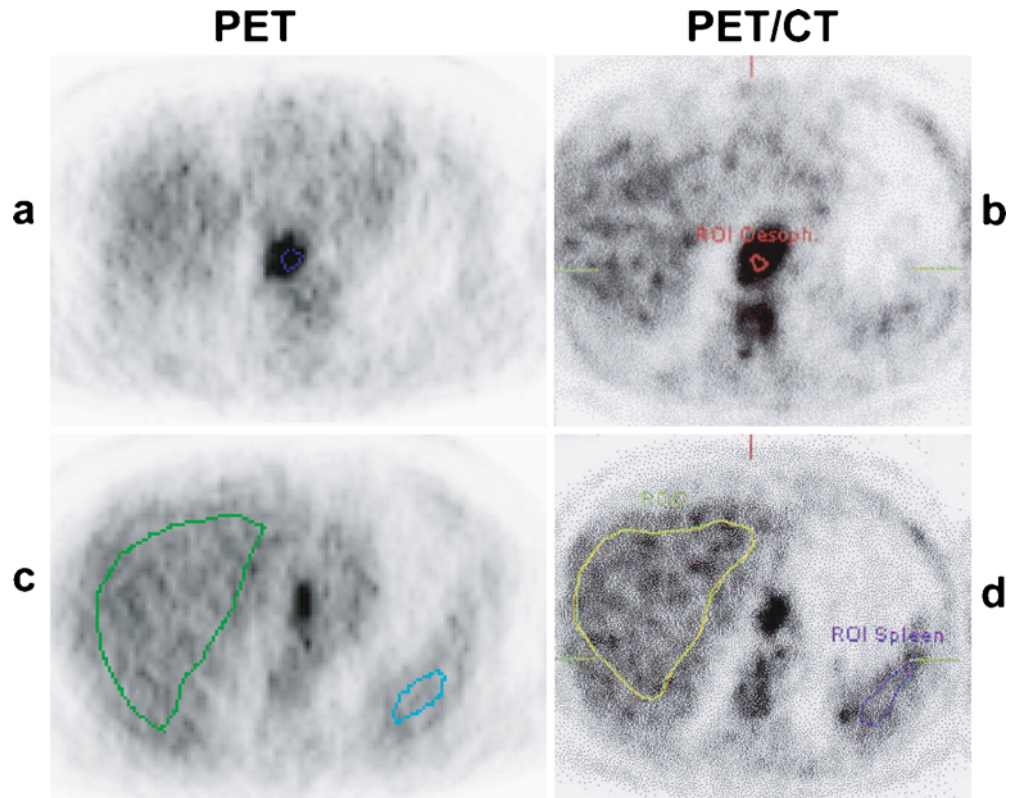
Phantom measurements were performed to complement patient findings. A body phantom with six spheres of increasing diameter (10 mm, 13 mm, 17 mm, 22 mm, 28 mm and 37 mm) containing water with  $41.6 \text{ kBq/ml}$  of FDG was imaged. The rest of the body phantom was filled with water containing  $5.2 \text{ kBq/ml}$  FDG. A cylinder filled with a non-active mixture of styrofoam and water of an average density of  $0.3 \text{ g/ml}$  was inserted into the centre of the phantom to simulate attenuation in lungs. To simulate scatter originating from regions outside the field of view, we attached a 70-cm-long solid cylindrical phantom containing a line filled with  $5.2 \text{ kBq/ml}$ . Acquisition was done first in PET/CT and then in PET using the same acquisition and reconstruction protocol as for the patients. For activity comparison, the time difference between the two scans was taken into account and decay correction was performed.

### *Data analysis*

Regions of interest (ROIs) were placed over matching locations in corresponding FDG images of suspected tumour lesions and organs (Fig. 1). To calculate SUVs for suspected tumour lesions, the axial slice with the maximum SUV of the lesion was first located automatically using standardised software for images of both scanners. An isocontour ROI of 75% around the maximum was then created to calculate mean SUVs. To determine the SUVs in organs in the two images, ROIs were placed in an anatomically corresponding central axial slice through the organ in question (brain, lung, liver, spleen and vertebral bone), delineating the shape of the organ but not including edge pixels. We compared both the mean (average of all pixels within the ROI) and maximum (hottest single pixel within the ROI) SUV in the two PET datasets for each patient. Lesions were grouped according to location (near to versus distant from the diaphragm).

Concerning data analysis of the phantom studies, volumes of interest with a diameter 90% of the sphere's diameter were centered in each sphere, and the average and maximum activity concentrations were calculated for both CT-corrected and germanium-corrected images. In the cold cylinder an ROI was placed in the slice with the body phantom's maximum diameter, and the average and maximum activity concentrations were determined.

**Fig. 1.** **a, b** ROI definition for lesions in PET (**a**) and PET/CT (**b**). An isocontour ROI (75% of maximum) was placed in the slice in which the lesion (here, oesophageal cancer) showed the maximum SUV in the respective images. **c, d** ROI definition for organs in PET (**c**) and PET/CT (**d**). ROIs were placed in an anatomically corresponding central axial slice through the organ, delineating the shape of the organ but not including edge pixels



#### Statistical analysis

Data are expressed as mean±standard deviation (SD). Multiple linear regression analysis was performed, taking the  $\Delta t$  (the time difference between the two scans) corresponding to each measurement as a covariate, in order to correct for  $\Delta t$  and to determine the correlation between maximum and mean SUVs obtained in organs and suspected tumour lesions.  $Z$  transformation was applied to each value and the  $z$  score was calculated according to the formula:

$$(SUV - \text{mean SUV}) / \text{standard deviation}.$$

For comparison between values derived from the CT and  $^{68}\text{Ge}$  attenuation-corrected PET data sets,  $\Delta t$  was taken into account and the 95% confidence interval for the coefficient of the multiple linear regression analysis was used. For comparison of the phantom data, paired Student's  $t$  test was used.

Statistical analysis was done with SPSS.

#### Results

Overall, the maximum and mean SUVs obtained from PET and PET/CT did correlate significantly and to a similar degree in both the patients who had stand-alone PET as the first scan ( $r=0.97$ ,  $p<0.001$ ) and those who had it as the second scan ( $r=0.96$  for  $SUV_{\max}$  and  $r=0.97$  for  $SUV_{\text{mean}}$ ,  $p<0.001$  in each case). SUVs were always higher in the second scan ( $p<0.05$ , Fig. 2).

#### Comparison of lesion SUVs according to location

A total of 46 lesions were analysed. Twenty of these had been scanned first with PET and then with PET/CT and 26 in the opposite order. Twenty-three were located in the oesophagus, 14 in mediastinal and hilar lymph nodes, five in the lungs, two in the liver and two in soft tissue. Both the maximum and the mean SUVs correlated significantly between stand-alone PET and PET/CT images (partial correlation coefficient  $r=0.9$  and  $r=0.92$ , respectively,  $p<0.001$ ). No systematic difference in  $\Delta t$  corrected absolute values was observed (Table 1, Fig. 3).

Fourteen lesions were located near to the diaphragm. Seven had been scanned first with PET and seven first with PET/CT. The partial correlation coefficients of maximum and mean SUVs calculated from PET and PET/CT were  $r=0.97$ ,  $p<0.001$  and  $r=0.97$ ,  $p<0.001$ , respectively. The mean  $SUV_{\max}$  values were slightly higher with PET/CT than with PET, but when comparing the  $\Delta t$  corrected absolute values the difference was not statistically significant (Table 1, Fig. 3). Thirty-two lesions were located distant from the diaphragm. Of these, 14 were scanned first with PET, while 18 were scanned first with PET/CT. The partial correlation coefficients of maximum and mean SUVs calculated from PET and PET/CT were  $r=0.87$ ,  $p<0.001$  and  $r=0.89$ ,  $p<0.001$ , respectively, and no differences were revealed when comparing the  $\Delta t$  corrected values of the mean  $SUV_{\max}$  and mean  $SUV_{\text{mean}}$  (Table 1).

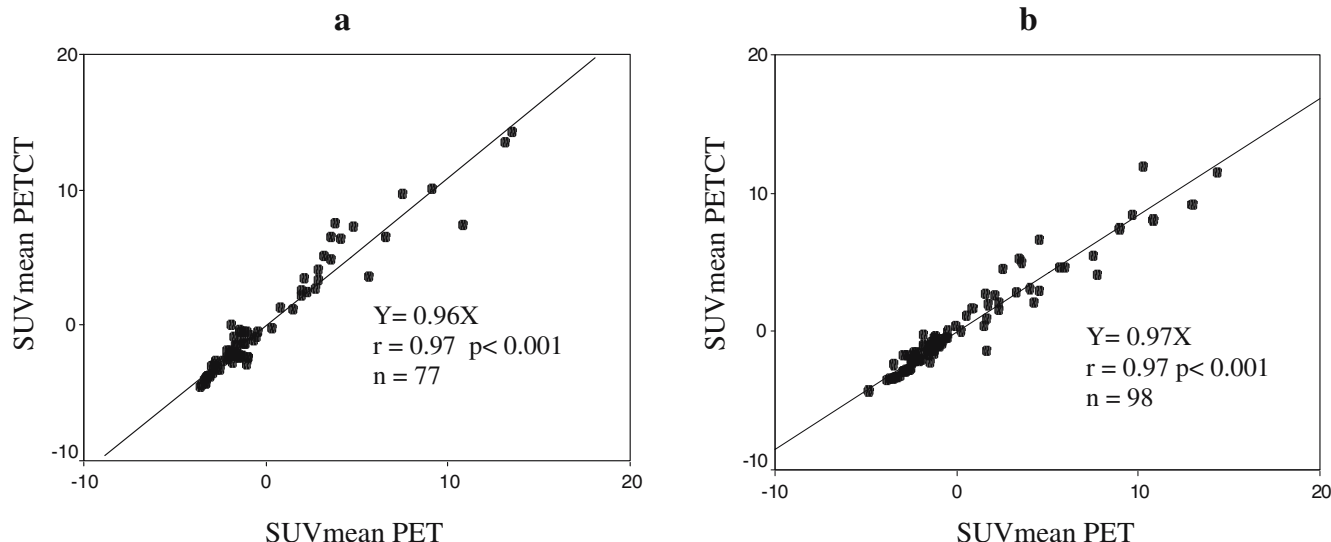


**Fig. 2.** Partial regression plot of the z-transformed  $SUV_{mean}$  measured in organs and lesions using the standardised coefficient for the equation of the fitting line in **a** patients scanned first with PET and then with PET/CT and **b** patients scanned first with PET/

CT and then with PET. A significant correlation is seen in both cases. Comparison of the data, taking  $\Delta t$  into account, revealed higher SUVs in the second scans in each case ( $p < 0.05$ )

*Comparison of SUVs in organs*

Overall, there was a significant correlation between  $\Delta t$ -corrected organ SUVs from PET and PET/CT (mean  $SUV_{max} r = 0.96, p < 0.001$ ; mean  $SUV_{mean} r = 0.95, p < 0.001$ ). Results for different organs are shown in Table 2. In the lungs, SUVs calculated from PET were higher (mean  $SUV 0.45 \pm 0.1$ ) than those calculated from PET/CT (mean  $SUV 0.34 \pm 0.1$ ) but the difference was not statistically significant. In bone tissue, SUVs were higher with PET/CT ( $SUV_{mean} 2.4 \pm 0.8$ ) than with PET ( $SUV_{mean} 2.1 \pm 0.5$ ), though again, the difference did not reach statistical significance. This was also true for the SUVs calculated in brain. In liver and spleen, SUVs calculated from PET were higher than those calculated from PET/CT ( $p < 0.05$ ).

*Phantom data*

Measured maximum and mean activity concentrations in germanium-corrected and CT-corrected images correlated significantly ( $r = 0.99, p < 0.001$ ; Fig. 4). Overall, no signif-

icant difference was observed when comparing these values ( $t$  test:  $p = 0.68$  for maximum activity concentrations and  $p = 0.63$  for mean activity concentrations). The  $\mu$  value determined in the cylinder imitating lung tissue attenuation was 15% higher with  $^{68}Ge$  transmission scan than with PET/CT (Table 3).

**Discussion**

In summary, our results demonstrate that SUVs calculated from PET/CT correlate significantly with those derived from stand-alone PET. When the values are compared with a method that takes into account the confounding effect of time-varying uptake, no significant differences are calculated. These data suggest that PET/CT can substitute for stand-alone PET for quantitative metabolic monitoring of tumour therapy response. Thresholds established from stand-alone PET may be transferred to the PET/CT setting. It is of note that in our setting of two successive scans on both systems, SUVs were always higher in the second scan (Fig. 2), which is consistent with continuous metabolic

**Table 1.** Results of the comparison of the calculated maximum and mean SUVs in all lesions, grouped according to their location

Lesions	n	Mean $SUV_{max} \pm SD$		r	Significant difference at $p < 0.05$	Mean $SUV_{mean} \pm SD$		r	Significant difference at $p < 0.05$
		PET	PET/CT			PET	PET/CT		
All lesions	46	10.43±5.1	10.38±5.2	0.9, $p < 0.001$	n.s.	8.54±4.3	8.49±4.2	0.92, $p < 0.001$	n.s.
Paradiaphragmatic	14	11.3±4.8	12.4±4.6	0.97, $p < 0.001$	n.s.	9.5±3.9	10.2±3.6	0.97, $p < 0.001$	n.s.
Distant from diaphragm	32	9.8±4.9	9.3±5.1	0.87, $p < 0.001$	n.s.	7.2±4.0	7.0±4.2	0.89, $p < 0.001$	n.s.

r partial correlation coefficient, p significance level, SD standard deviation, n.s. non-significant



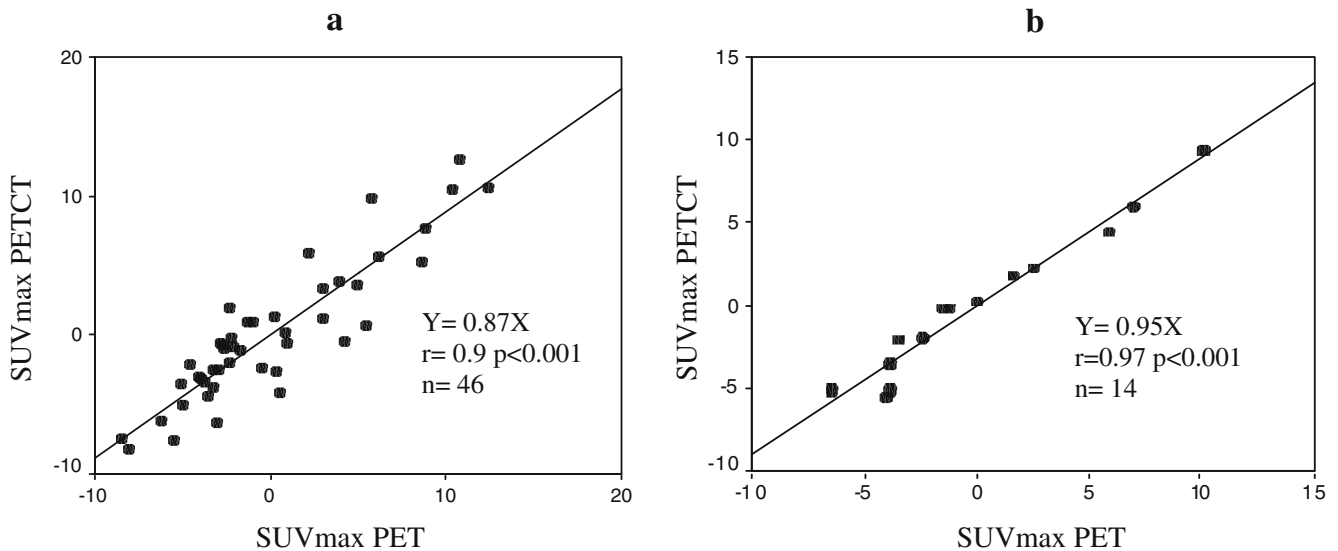


**Fig. 3.** Partial regression plot of the  $z$ -transformed  $SUV_{max}$  using the standardised coefficient for the equation of the fitting line in **a** all lesions and **b** the paradiaphragmatic lesions. A significant correlation

is seen in both cases. Comparison of the data, taking  $\Delta t$  into account, revealed no significant differences between the first and second scans in either case

trapping of the tracer. To compensate for this systematic error, we studied two groups in which the sequence of scans was changed and compared the SUVs with a method that takes into account the confounding effect of time-varying uptake. Some minor differences between the two methods, however, were observed in our study. This suggests that it is preferable to use the same system, either stand-alone PET or PET/CT, in an individual patient when a protocol of repetitive scans for serial therapy monitoring is applied.

#### *SUVs in tumour lesions*

In a study examining the effect of ROI definition on the accuracy of the estimated SUVs, Boellaard et al. [20] demonstrated that the maximum pixel value is the best choice for determining the activity concentration in a lesion. We recorded both  $SUV_{mean}$  and  $SUV_{max}$ , but for comparison of the data concerning the lesions the  $SUV_{max}$  is appropriate.

Differences in the temporal and spatial resolution of the two transmission scans could possibly lead to differences

in the calculated SUVs. PET and conventional transmission scan are acquired over several minutes, both reflecting the average breathing position of the patient. CT is acquired over a few seconds, reflecting a snap shot of a lesion in motion for only a part of the respiratory cycle. This can lead to misalignment between the PET and the CT scan and to possible application of wrong attenuation coefficients. In previous studies, artefacts originating from such misalignments have been described [21–23]. Visvikis et al. [24] showed that a mismatch between PET and CT due to respiration may degrade the quality of attenuation correction of PET images and consequently produce inaccurate SUVs. In our study, we observed a good overall correlation for lesion SUVs between PET and PET/CT. We applied a PET/CT breathing protocol which is a combination of approaches suggested by Goerres et al. [21] and Beyer et al. [22] to result in the best match between PET and CT. Patients were asked to breathe shallowly during the whole PET/CT acquisition and to hold their breath during the CT acquisition of the thorax and the upper abdomen. Our data indicate that this approach yields robust CT alignment for attenuation correction and subsequent quantification.

**Table 2.** Results of the comparison of the calculated maximum and mean SUVs in normal organs

Organ	$n$	Mean SUV $\pm$ SD, PET	Mean SUV $\pm$ SD, PET/CT	Significant difference at $p<0.05$	Max. SUV $\pm$ SD, PET	Max. SUV $\pm$ SD, PET/CT	Significant difference at $p<0.05$
Lung	35	0.45 $\pm$ 0.1	0.34 $\pm$ 0.1	n.s.	0.74 $\pm$ 0.2	0.64 $\pm$ 0.28	n.s.
Liver	30	2.17 $\pm$ 0.45	2.19 $\pm$ 0.43	$p<0.05$	3.3 $\pm$ 0.8	3.2 $\pm$ 0.7	$p<0.05$
Spleen	26	1.8 $\pm$ 0.37	1.9 $\pm$ 0.34	$p<0.05$	2.4 $\pm$ 0.5	2.45 $\pm$ 0.5	$p<0.05$
Bone	34	2.1 $\pm$ 0.53	2.4 $\pm$ 0.82	n.s.	2.7 $\pm$ 0.8	2.9 $\pm$ 1.0	n.s.
Brain	10	5.1 $\pm$ 1.2	5.9 $\pm$ 1.6	n.s.	8.7 $\pm$ 2.1	10.2 $\pm$ 3.1	n.s.

*SD* standard deviation, *n.s.* non-significant

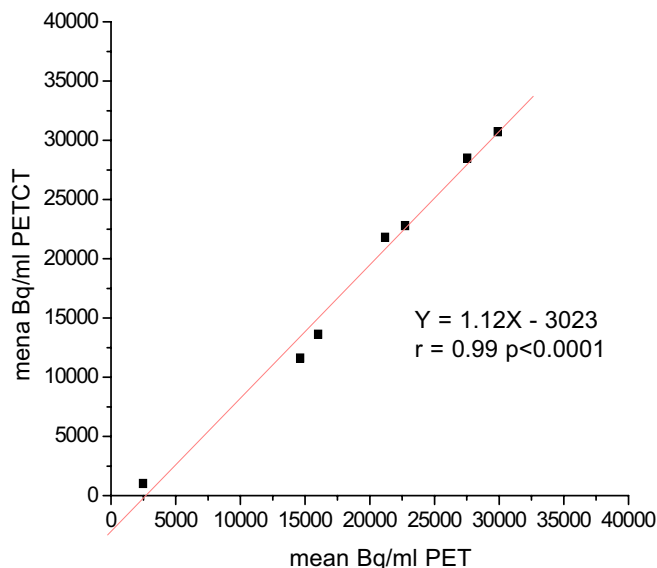


**Fig. 4.** Phantom measurement. Regression analysis of the mean activity concentrations (Bq/ml) measured in the six hot spheres and in the cold cylinder with PET and PET/CT. There was a significant correlation of the measured activities. Higher activity was measured in the cold cylinder with PET than with PET/CT

In a study in which CT scans were acquired in different respiratory cycles in patients with lung lesions, Erdi et al. [25] demonstrated a variation of up to 30% in the calculated  $SUV_{max}$  depending on which “snap shot” CT was used for attenuation correction. We therefore distinguished between paradiaphragmatic lesions and those located distant from the diaphragm. The paradiaphragmatic region is subjected to the largest movements, which are relatively unidirectional and sized in centimetres [21, 26]. This could change the photon equivalent pathlength, and consequently affect the SUV. Despite that, the calculated SUVs in the two scans did correlate well and were not significantly different.

**Table 3.** Mean  $\mu$  values applied for attenuation correction in PET and PET/CT by the conventional  $^{68}\text{Ge}$  transmission scan (tx) for PET and the CT transmission scan for PET/CT in lung, soft tissue and bone

	$\mu$ values ( $\text{cm}^{-1}$ ; mean $\pm$ SD)	
	$^{68}\text{Ge}$ -tx	CT
Lung	0.026 $\pm$ 0.004	0.019 $\pm$ 0.005
Soft tissue	0.098 $\pm$ 0.0008	0.1 $\pm$ 0.002
Bone	0.099 $\pm$ 0.004	0.116 $\pm$ 0.002
Imitated lung (phantom)	0.033	0.028

The last row shows the  $\mu$  value applied for the cylinder placed in the centre of the phantom.  
SD standard deviation

In this study we compared our routinely used HR+ clinical protocol (2D acquisition mode, no scatter correction; for details, see [Materials and methods](#) section) with the clinical protocol for the PET/CT scanner in order to evaluate whether established threshold values for therapy monitoring can be transferred to scans acquired with PET/CT. The HR+ acquisition protocol was established in our institution in 2D mode without application of scatter correction because the accuracy of the implemented 2D scatter correction had been shown to be limited in whole-body scans (validation tests performed in our institution). Thus we decided years ago to use a protocol without scatter correction for treatment monitoring, and the threshold values were established in 2D acquisition mode without application of any scatter correction. Changing the protocol for the HR+ stand-alone PET would have been misleading because the acquisition would then not have been similar to that used in our clinical oncological studies.

#### *SUVs in normal tissue*

We compared the calculated SUVs in various background tissues, including brain, lung, liver, spleen and vertebral bone. For all organs the pooled data showed a significant correlation between the two acquisition techniques. Additionally we determined the attenuation coefficients ( $\mu$  values) applied for attenuation correction in PET and PET/CT for lung, soft tissue and bone (Table 3).

Tendencies towards differences were observed in lung and in bone. The SUVs calculated in lung showed a tendency to be higher in PET than in PET/CT. Two major factors may account for the differences observed in the lungs. Firstly, as the aim of our study was to compare the SUVs calculated from our routine clinical images, we used the acquisition protocols applied in routine clinical work, which include scatter correction of 3D PET/CT acquisition [19] but no scatter correction of 2D stand-alone PET acquisition. The fraction of scattered photons of all detected events in 2D acquisition is approximately 10–15% [27] and this could have contributed to the higher activity measured in the lung in PET. Secondly, determination of the applied  $\mu$  values for attenuation correction shows that in comparison to the values derived from the conventional transmission scan, the values calculated from the CT scan are lower (mean difference in the mean  $\mu$  values of approximately 27%), possibly resulting in an underestimation of the activity calculated in the lungs in PET/CT. Given the aim of this study, determination of the exact contribution of the differences in the  $\mu$  values to the calculated SUVs was beyond the limits of the study. However, for the daily clinical use of PET/CT it is important that no significant differences were calculated in the lung when the data were compared with a method that takes into account the confounding effect of time-varying uptake. This result is in line with the results of the study of Nakamoto et al. [28].

The SUVs calculated in bone tissue tended to be higher in PET/CT than in PET (Table 2). The CT-derived mean  $\mu$

values based on a bilinear transformation were approximately 14% higher than the  $\mu$  values calculated with the conventional transmission scan (Table 3), providing a possible explanation for this tendency. Nakamoto et al. [28] found significant differences between the activity concentrations calculated in bone with conventional and with CT attenuation correction. They hypothesised that the differences in the interaction of X-rays and 511-keV photons with bony tissue lead to errors in the conversion of bone CT values to 511-keV attenuation values. To prove this hypothesis was beyond the limits of our study. However, the observed tendency towards higher SUVs in bony tissue in PET/CT is indeed based on the higher attenuation coefficients determined from CT.

Recently, Papathanassiou et al. [29] examined PET images corrected for attenuation with  $^{137}\text{Cs}$  transmission measurement and with CT in order to compare the appearance of the liver and the calculated SUVs in this organ and in liver lesions when using the two attenuation correction methods. In contrast to our results, they found significantly higher SUVs in the liver and in the liver lesions when the image was CT corrected.

The results of our study are in part not in line with the results of similar studies using other PET/CT devices [28, 29] concerning the differences in calculated SUVs in bone [28] and liver [29]. However, comparison of PET/CT data obtained with devices from different manufacturers is restricted by the fact that the same function is not applied to transform the HU to 511-keV attenuation values [30]. Additionally, differences in the reconstruction algorithms as well as differences in tomograph technologies and geometries that affect measurement accuracy [27] may have contributed to the described disagreements.

#### *Limitations of the study*

The aim of this study was to compare approaches for tumour metabolic quantification using clinically established imaging protocols for stand-alone PET and PET/CT. As a consequence, differences with regard to the presence/absence of scatter correction need to be taken into account, as discussed above. However, all reconstruction parameters were identical; this is important, as Schöder et al. [27] reported that differences in SUVs of more than 25% were solely attributable to differences in image reconstruction.

In conclusion, our study demonstrates that there is a significant correlation between the SUVs calculated in lesions and organs using stand-alone PET and PET/CT. Treatment response evaluation can thus be carried out using PET/CT in a manner similar to PET with conventional attenuation correction. Owing to the additional accurate anatomical information provided by the CT component of PET/CT, functional and morphological response criteria could be combined in the future to yield a new integrative treatment response factor.

## References

- Gambhir SS, Czernin J, Schwimmer J, Silverman DH, Coleman RE, Phelps ME. A tabulated summary of the FDG PET literature. *J Nucl Med* 2001;42:1–93.
- Czernin J, Phelps ME. Positron emission tomography scanning: current and future applications. *Annu Rev Med* 2002;53:89–112.
- Römer W, Hanauske AR, Ziegler S, Thodtmann R, Weber W, Fuchs C, et al. Positron emission tomography in non-Hodgkin's lymphoma: assessment of chemotherapy with fluorodeoxyglucose. *Blood* 1998;91:4464–71.
- Schelling M, Avril N, Nahrig J, Kuhn W, Romer W, Sattler D, et al. Positron emission tomography using [ $^{18}\text{F}$ ]fluorodeoxyglucose for monitoring primary chemotherapy in breast cancer. *J Clin Oncol* 2000;18(8):1689–95.
- Weber WA, Petersen V, Schmidt B, Tyndale-Hines L, Link T, Peschel C, et al. Positron emission tomography in non-small-cell lung cancer: prediction of response to chemotherapy by quantitative assessment of glucose use. *J Clin Oncol* 2003;21(14):2651–7.
- Kostakoglu L, Coleman M, Leonard JP, Kuji I, Zoe H, Goldsmith SJ. PET predicts prognosis after 1 cycle of chemotherapy in aggressive lymphoma and Hodgkin's disease. *J Nucl Med* 2002;43(8):1018–27.
- Haioun C, Itti E, Rahmouni A, Brice P, Rain JD, Belhadj K, et al. [ $^{18}\text{F}$ ]fluoro-2-deoxy-D-glucose positron emission tomography (FDG-PET) in aggressive lymphoma: an early prognostic tool for predicting patient outcome. *Blood* 2005;106(4):1376–81.
- Becherer A, Mitterbauer M, Jaeger U, Kalhs P, Greinix HT, Karanikas G, et al. Positron emission tomography with [ $^{18}\text{F}$ ]2-fluoro-D-2-deoxyglucose (FDG-PET) predicts relapse of malignant lymphoma after high-dose therapy with stem cell transplantation. *Leukemia* 2002;16(2):260–7.
- Wieder HA, Brucher BL, Zimmermann F, Becker K, Lordick F, Beer A, et al. Time course of tumour metabolic activity during chemoradiotherapy of esophageal squamous cell carcinoma and response to treatment. *J Clin Oncol* 2004;22(5):900–8.
- Brucher BL, Weber W, Bauer M, Fink U, Avril N, Stein HJ, et al. Neoadjuvant therapy of esophageal squamous cell carcinoma: response evaluation by positron emission tomography. *Ann Surg* 2001;233(3):300–9.
- Weber WA, Ott K, Becker K, Dittler HJ, Helmberger H, Avril NE, et al. Prediction of response to preoperative chemotherapy in adenocarcinomas of the esophagogastric junction by metabolic imaging. *J Clin Oncol* 2001;19:3058–65.
- Bailey DL. Transmission scanning in emission tomography. *Eur J Nucl Med* 1998;25(7):774–87.
- Kinahan PE, Townsend DW, Beyer T, Sashin D. Attenuation correction for a combined 3D PET/CT scanner. *Med Phys* 1998;25(10):2046–53.
- Young H, Baum R, Cremerius U, Herholz K, Hoekstra O, Lammertsma AA, et al. Measurement of clinical and subclinical tumour response using [ $^{18}\text{F}$ ]fluorodeoxyglucose and positron emission tomography: review and 1999 EORTC recommendations. European Organization for Research and Treatment of Cancer (EORTC) PET Study Group. *Eur J Cancer* 1999;35:1773–82.
- Hamacher K, Coenen HH, Stocklin G. Efficient stereospecific synthesis of no-carrier-added 2-[ $^{18}\text{F}$ ]fluoro-2-deoxy-D-glucose using aminopolyether supported nucleophilic substitution. *J Nucl Med* 1986;27(2):235–8.
- Herzog H, Tellmann L, Hocke C, Pietrzyk U, Casey M, Kuwert T. NEMANU2-2001 guided performance evaluation of four Siemens ECAT PET-scanners. Nuclear Science Symposium Conference Record, 2003 IEEE;4:2836–8.

17. Xu EZ, Mullani NA, Gould KL, Anderson WL. A segmented attenuation correction for PET. *J Nucl Med* 1991;32(1):161–5.
18. Meikle SR, Dahlbom M, Cherry SR. Attenuation correction using count-limited transmission data in positron emission tomography. *J Nucl Med* 1993;34(1):143–50.
19. Watson CC. New, faster, image-based scatter correction for 3D PET. *IEEE Trans Nucl Sci* 2000;47(4):1587–94.
20. Boellaard R, Krak NC, Hoekstra OS, Lammertsma AA. Effects of noise, image resolution, and ROI definition on the accuracy of standard uptake values: a simulation study. *J Nucl Med* 2004;45(9):1519–27.
21. Goerres GW, Kamel E, Heidelberg TN, Schwitter MR, Burger C, von Schulthess GK. PET-CT image co-registration in the thorax: influence of respiration. *Eur J Nucl Med Mol Imaging* 2002;29(3):351–60.
22. Beyer T, Antoch G, Blodgett T, Freudenberg LF, Akhurst T, Mueller S. Dual-modality PET/CT imaging: the effect of respiratory motion on combined image quality in clinical oncology. *Eur J Nucl Med Mol Imaging* 2003;30(4):588–96.
23. Osman MM, Cohade C, Nakamoto Y, Wahl RL. Respiratory motion artifacts on PET emission images obtained using CT attenuation correction on PET-CT. *Eur J Nucl Med Mol Imaging* 2003;30(4):603–6.
24. Visvikis D, Costa DC, Croasdale I, Lonn AH, Bomanji J, Gacinovic S, et al. CT-based attenuation correction in the calculation of semi-quantitative indices of [ $^{18}\text{F}$ ]FDG uptake in PET. *Eur J Nucl Med Mol Imaging* 2003;30(3):344–53.
25. Erdi YE, Nehmeh SA, Pan T, Pevsner A, Rosenzweig KE, Mageras G, et al. The CT motion quantitation of lung lesions and its impact on PET-measured SUVs. *J Nucl Med* 2004;45(8):1287–92.
26. Goerres GW, Kamel E, Seifert B, Burger C, Buck A, Hany TF, et al. Accuracy of image coregistration of pulmonary lesions in patients with non-small cell lung cancer using an integrated PET/CT system. *J Nucl Med* 2002;43(11):1469–75.
27. Schöder H, Erdi YE, Chao K, Gonen M, Larson SM, Yeung HW. Clinical implications of different image reconstruction parameters for interpretation of whole-body PET studies in cancer patients. *J Nucl Med* 2004;45:559–66.
28. Nakamoto Y, Osman M, Cohade C, Marshall LT, Links JM, Kohlmyer S, et al. PET/CT: comparison of quantitative tracer uptake between germanium and CT transmission attenuation-corrected images *J Nucl Med* 2002;43(9):1137–43.
29. Papathanassiou D, Becker S, Amir R, Meneroux B, Liehn JC. Respiratory motion artefact in the liver dome on FDG PET/CT: comparison of attenuation correction with CT and a caesium external source. *Eur J Nucl Med Mol Imaging* 2005;32(12):1422–8.
30. Burger C, Goerres G, Schoenes S, Buck A, Lonn AH, Von Schulthess GK. PET attenuation coefficients from CT images: experimental evaluation of the transformation of CT into PET 511-keV attenuation coefficients. *Eur J Nucl Med Mol Imaging* 2002;29(7):922–7.